ACS Catalysis

pubs.acs.org/acscatalysis Research Article

Engineering the ZrO_2–Pd Interface for Selective CO_2 Hydrogenation by Overcoating an Atomically Dispersed Pd Precatalyst

Yuan-Peng Du, Ali M. Bahmanpour, Luka Milošević, Florent Héroguel, Mounir D. Mensi, Oliver Kröcher, and Jeremy S. Luterbacher*

Cite This: *ACS Catal.* 2020, 10, 12058–12070 Read Online

ACCESS | Metrics & More | Article Recommendations | Supporting Information

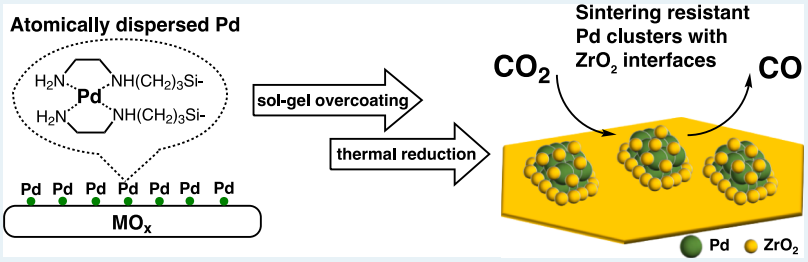

ABSTRACT: Tailoring the interfacial sites between metals and metal oxides can be an essential tool in designing heterogeneous catalysts. These interfacial sites play a vital role in many renewable applications, for instance, catalytic CO_2 reduction. Postsynthesis deposition of metal oxide on supported metal catalysts can not only create such interfacial sites but also prevent particle sintering at high temperature. Here, we report a sol–gel-based strategy to synthesize an atomically dispersed "precatalyst". In contrast to the deposition on catalysts containing preformed nanoparticles, overcoating this material before reductive treatment can inhibit particle growth during thermal activation steps, yielding highly accessible, sintering-resistant Pd clusters that are less than 2 nm in diameter. This synthetic approach allows us to engineer interfacial sites while maintaining high metal accessibility, which was difficult to achieve in previous overcoated materials. Notably, engineering the Pd–ZrO_2 interface into an inverted interface with an amorphous ZrO_2 overcoat might facilitate a C–O cleavage route instead of a mechanism containing a bicarbonate intermediate during CO_2 hydrogenation. We also observed that carbon deposition occurring on methanation sites could be a key factor for improving CO selectivity. Alteration of the reaction pathway, along with the deactivation of certain sites, led to 100% CO selectivity on the ZrO_2@Pd/ZrO_2 catalyst. This work demonstrated that overcoated materials could represent a promising class of heterogeneous catalysts for selective CO_2 conversion over noble metals, which have higher rates and thermal stability compared to state-of-the-art Cu-based catalysts.

KEYWORDS: *sol–gel chemistry, heterogeneous catalysis, catalyst overcoating, CO_2 hydrogenation, metal support interface*

INTRODUCTION

Heterogeneous catalysis is an essential workhorse of the chemical industry and for the production of bulk commodity chemicals.[1] Since the last decade, focus has been placed on identifying different active sites and gaining new insights into structure–reactivity relations in order to design more selective catalysts for converting renewable feedstocks (*e.g.*, biomass and CO_2). The importance of metal–metal oxide interfaces has been recognized for the catalytic transformation of CO_2.[2−4] Such interfacial sites can be tailored by controlling the size of nanoparticles, through the occurrence of *in situ* encapsulation with strong metal support interactions and postsynthesis modification.[5] Postsynthesis *via* metal oxide overcoating is a particularly attractive set of methods because of the flexibility of metal oxides that can be used. Additionally, the metal oxide overcoat can inhibit the sintering of nanoparticles during catalytic reactions, thus lengthening the catalysts' life time.[6,7] Another intriguing characteristic of overcoated catalysts is the formation of a "metal oxide overcoat–metal–metal oxide support" interface, as opposed to the uncoated "metal–metal oxide support" configuration, which sometimes leads to higher stabilities and/or different catalytic properties.[8,9] Because of this unique catalyst structure, overcoated catalysts have been referred to as "inverted catalysts".[10] Creating interfacial sites using overcoating strategies also has the potential to lower the cost during catalyst synthesis because nanoparticles can be supported on a less expensive support with high surface area (*e.g.*, silica) and be further functionalized with another metal

Received: May 14, 2020
Revised: August 13, 2020
Published: September 16, 2020

https://dx.doi.org/10.1021/acscatal.0c02146
ACS Catal. 2020, 10, 12058–12070

Scheme 1. Coordination Chemistry of a Silane with the Ethylenediamine Functionality and Pd and Its Use in the Synthesis of Ultrasmall Pd Clusters with a ZrO_2 Interface Using Kinetically Controlled Sol−Gel Overcoating

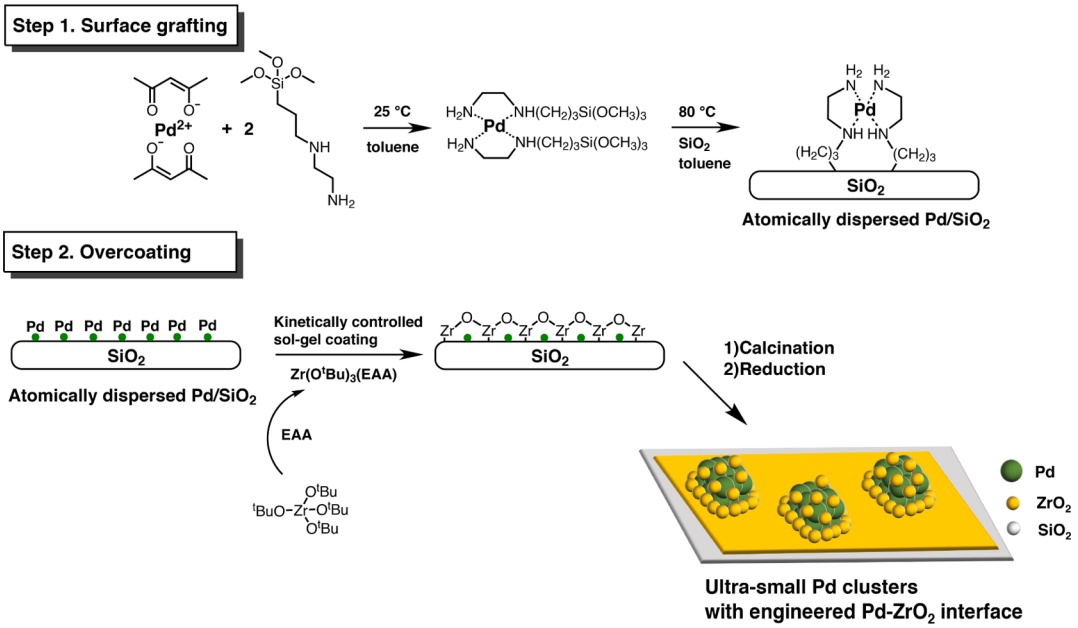

oxide overcoat. However, postdeposition is still facing several challenges. For instance, metal oxide overcoats usually impede the accessibility of active sites, which could be due to the dense texture of the overcoat and/or the interactions between metal oxide precursors and nanoparticles.[11−13] Moreover, current metal oxide deposition techniques often rely on gas-phase deposition techniques such as atomic layer deposition (ALD).[14] When overcoating catalyst powders with high surface area, large excess quantities of precursors and long exposure time are sometimes needed to overcome mass transfer limitations. The need for a specialized high vacuum instrument also greatly increases the cost. In addition, although the highly conformal and dense films produced by ALD are ideal for specific applications such as electronics, they are not necessarily adapted to catalyst synthesis, where more porous overcoats with improved accessibility might be more desirable. In this context, we have developed several liquid-phase methods that might lower the costs of catalyst overcoating, including an approach relying on stoichiometric injection of metal alkyl precursors in the liquid phase, which produced the overcoats that could match the quality and conformality of ALD,[15] and others using sol−gel precursors that led to conformal but less dense overcoat.[16−18] Nevertheless, the loss of active sites after coating still remains a significant challenge to prepare an active catalyst, not merely in the materials prepared by ALD but also for catalysts with less dense overcoats synthesized using wet-chemistry methods.[6,19]

Here, we report a sol−gel-based approach to prepare an atomically dispersed "precatalyst" by combining the surface reaction of alkoxysilane and the coordination chemistry of palladium and ethylenediamine (en). Liquid-phase-based overcoating was then performed on this precatalyst to restrain the growth of the Pd particle during thermal treatments and engineer a new metal oxide−Pd interface. The resulting overcoated catalysts have highly accessible sub-nanometer Pd clusters with an engineered metal oxide interface. We found that the ZrO_2−Pd interface that formed on the relatively inactive SiO_2 surface substantially increased the activity toward CO_2 activation. We also observed an altered CO_2 hydrogenation mechanism on the new ZrO_2−Pd interface, which is distinct from that on the uncoated Pd−ZrO_2 interface. Although maintaining high conversion, the altered mechanism leads the reaction over the ZrO_2@Pd/ZrO_2 catalyst to achieve 100% CO selectivity. The overcoated catalyst is also more sintering-resistant than the uncoated Pd/ZrO_2. The enhancement of both catalyst selectivity and stability makes this synthetic approach highly promising in designing catalysts for CO_2 conversion.

RESULTS AND DISCUSSION

Catalyst Synthesis Using Atomically Dispersed Precatalysts and Metal Oxide Overcoats. Ethylenediamine is a bidentate ligand that can form complexes with noble metals.[20,21] A combination of molecules containing this chelating functionality and an alkoxysilane has been used to prepare SiO_2-supported metal catalysts through sol−gel processing.[22] Our synthesis approach relies on the same chemistry. Specifically, the chelated Pd was grafted on the SiO_2 surface through the condensation of Si-$(OCH_3)_3$ with silica's surface hydroxyl groups (step 1, Scheme 1), which produced an atomically dispersed Pd/SiO_2 [Pd$(en)_2$/SiO_2]. The completion of grafting could be simply observed from the color change of silica and the reaction medium (Figure S1). Diffuse reflectance infrared Fourier transform spectroscopy (DRIFTS) analysis of the resulting material revealed the presence of two bands at 2937 and 2883 cm^{-1} that could be assigned to C−H stretching, which confirmed the presence of the Pd complex on the silica surface (Figure S2).[23] Pd$(en)_2$/SiO_2 was then overcoated with ZrO_2 using a kinetically controlled sol−gel method similar to what we had previously reported for alumina and niobia.[16,24] Specifically, we slowed down the hydrolysis and condensation rates of Zr(*t*-BuO)$_4$ by adding ethyl acetoacetate (EAA) to form a chelated ZrO_2 precursor.[25] The resulting kinetically controlled precursor was injected into a Stöber solution (*i.e.*, an ethanol solution containing targeted quantities of NH_3 and H_2O), which was

https://dx.doi.org/10.1021/acscatal.0c02146
ACS Catal. 2020, 10, 12058−12070

Table 1. Summary of the Characterization Results of Reference and Overcoated Catalysts

catalyst	loading[a] (%)	S_{BET} ($m^2 \cdot g^{-1}$)	$Pd_{surface}$[b] ($\mu mol \cdot g^{-1}$)	d_{Pd}[c] (nm)	dispersion[d] (%)
g-Pd/SiO_2	0.39	170.1	6.9	3.4	19
ZrO_2@Pd/SiO_2	0.28	162.1	9.9	N/A	38
Al_2O_3@Pd/SiO_2	0.32	170.9	12.0	1.4	40
ZrO_2@Pd/ZrO_2	0.34	76.8	22.1	N/A	70
Pd/Al_2O_3	0.4	164.1	13.4	2.6	36
Pd/ZrO_2	0.57	64.3	47.3	N/A	89

[a]Determined by ICP-OES. [b]Determined by CO chemisorption. Although CO with two- and threefold coordination may also be present, we still assume the stoichiometric ratio between Pd and CO to be 1. A discussion justifying the choice of this stoichiometric number is given in the Supporting Information. [c]Determined by STEM, Pd supported on ZrO_2 or with ZrO_2 overcoat cannot be observed because of the insufficient contrast. [d]Pd dispersion, calculated by $Pd_{surface}$/total Pd.

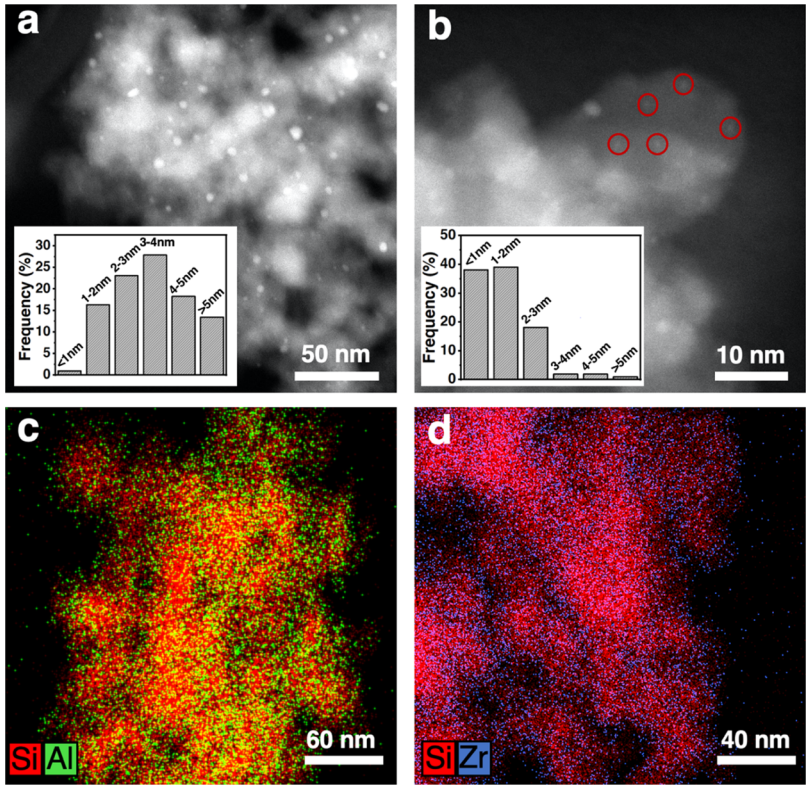

Figure 1. TEM images and Pd particle size distributions of (a) g-Pd/SiO_2 and (b) Al_2O_3@Pd/SiO_2 and EDX mappings of (c) Al_2O_3@Pd/SiO_2 and (d) ZrO_2@Pd/SiO_2. The sub-nanometer Pd clusters observed in panel b are highlighted by red circles.

mixed with dispersed Pd$(en)_2$/SiO_2, to grow a ZrO_2 overcoat (step 2, Scheme 1). Importantly, the Pd$(en)_2$ complex remained unreactive because of the strong interaction between ethylenediamine and Pd. Therefore, the Pd that was grafted on the surface did not leach when performing liquid-phase coating during which another chelating agent (EAA) was also present in solution. In addition to our presented method, an alternate method for immobilizing Pd using arginine was also reported where the amine group of arginine was used to coordinate Pd, and the resulting complex was anchored on the surface *via* the carboxylic acid group.[26] Nevertheless, such a Pd−arginine complex likely interacted with silica by electrostatic interaction rather than by covalent bonding. In this study, we grafted the Pd$(en)_2$ complex by forming a covalent siloxane linkage, which is more stable than electrostatic forces. We had also tried to overcoat an impregnated silica containing a strongly electrostatically adsorbed Pd complex,[27] but most of the Pd leached during the coating procedure, which was likely caused by the complexation between EAA (*i.e.*, one of our overcoating reagents) and Pd. Accordingly, we proposed that using an organo-functionalized silane could result in the most stable material that is compatible with kinetically controlled sol−gel coating. In the last step, the atomically dispersed precatalyst overcoated with ZrO_2 (ZrO_2@Pd$(en)_2$/SiO_2) was first calcined at 400 °C to remove any impurities containing C and N from the synthesis reagents and then reduced to form the final Pd catalyst by flowing H_2 at 400 °C. The same thermal treatments were also performed on uncoated Pd$(en)_2$/SiO_2 to form g-Pd/SiO_2 (where g stands for the material prepared from the grafted SiO_2) in order to compare the effect of the overcoat on the nanoparticle size distribution.

We first determined the dispersions of ZrO_2@Pd/SiO_2 and g-Pd/SiO_2 using CO chemisorption and inductively coupled plasma optical emission spectroscopy (ICP-OES). The Pd dispersion on ZrO_2@Pd/SiO_2 (38%, Table 1) was twice higher than that on g-Pd/SiO_2 (19%, Table 1). Scanning transmission electron microscopy (STEM) further confirmed a larger average Pd particle size for g-Pd/SiO_2 (3.4 nm, Figure 1a).

https://dx.doi.org/10.1021/acscatal.0c02146
ACS Catal. 2020, 10, 12058−12070

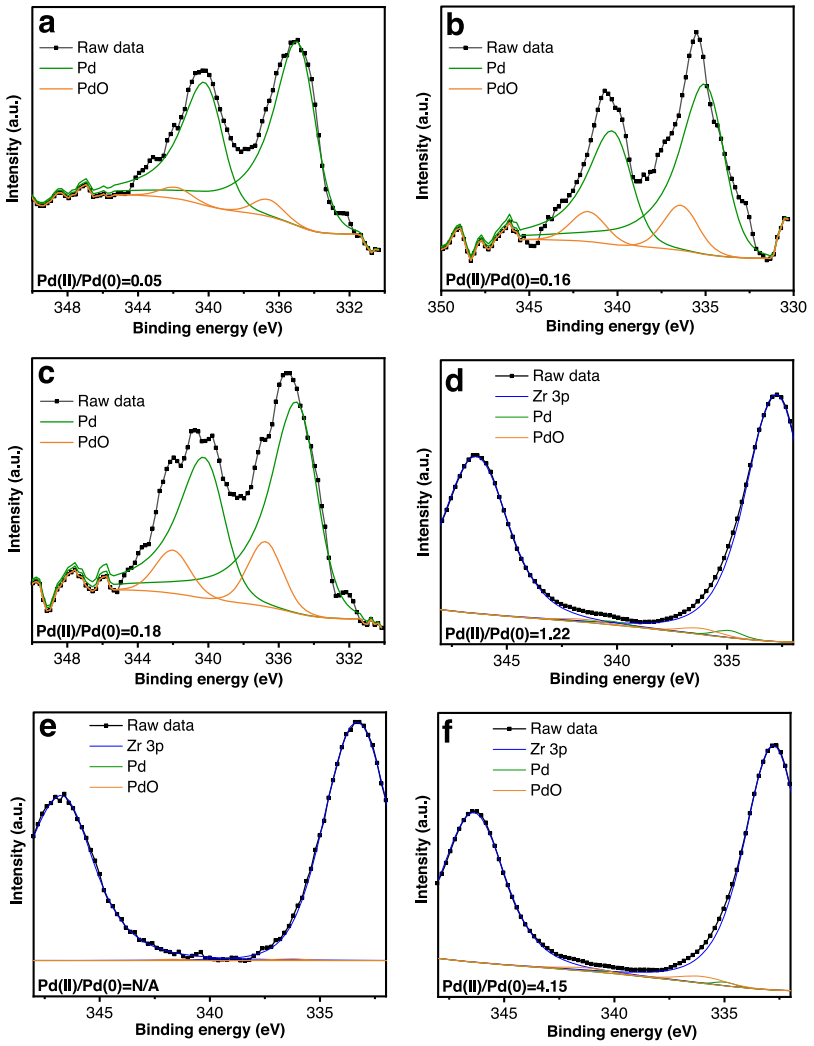

Figure 2. XPS spectra and deconvolution results for (a) g-Pd/SiO_2, (b) Pd/Al_2O_3, (c) Al_2O_3@Pd/SiO_2, (d) Pd/ZrO_2, (e) ZrO_2@Pd/SiO_2, and (f) ZrO_2@Pd/ZrO_2.

We were unable to observe Pd particles and measure the particle size distribution on ZrO_2@Pd/SiO_2 because of the poor contrast between Pd and ZrO_2 (Figure S3). Therefore, we prepared Al_2O_3@Pd/SiO_2 using a similar kinetically controlled approach,[16] as we expected that the higher contrast between Al_2O_3 and Pd would enable us to analyze Pd particles using STEM. Indeed, a much better contrast was obtained and many sub-nanometer Pd clusters were observed when analyzing Al_2O_3@Pd/SiO_2. STEM analyses showed that its average particle size was significantly smaller (1.4 nm) than that of g-Pd/SiO_2 (Figure 1b). The dispersion of Al_2O_3@Pd/SiO_2 was also obtained using CO chemisorption and ICP-OES. Because the dispersion of Al_2O_3@Pd/SiO_2 was very close to that of ZrO_2@Pd/SiO_2 (Table 1), we inferred that ZrO_2@Pd/SiO_2 also has similarly small Pd clusters. These results strongly suggested that the overcoat can inhibit the growth of Pd particles during thermal activation and further highlighted the potential of combining overcoating techniques and atomically dispersed materials for synthesizing sintering-resistant catalysts with high dispersion.[28,29] The energy-dispersive X-ray (EDX) mapping (Figure 1c,d) also showed that kinetically controlled sol−gel methods can uniformly grow both ZrO_2 and Al_2O_3 on high-surface-area SiO_2 (Aerosil 200), which is a more industrially relevant support. In contrast to a recently reported analogous approach, the strategy presented here does not require expensive organometallic complexes or an ALD instrument.[30] Although organometallic complexes are known precursors for preparing atomically dispersed catalysts, they are typically moisture sensitive, which is not compatible with sol−gel processes where water is present in the reaction media. $Pd(en)_2/SiO_2$ is fairly inert and can be stored in an ambient environment. This stable characteristic makes $Pd(en)_2/SiO_2$ an ideal precatalyst for synthesizing catalysts with a metal oxide overcoat−metal−metal oxide support configuration, which may possess different catalytic properties from that of supported catalysts with regular metal−metal oxide interfaces. Here, we took advantage of the stabilization effects of the overcoat and illustrated the use of $Pd(en)_2/SiO_2$ for synthesizing ultrasmall Pd clusters with Al_2O_3−Pd or ZrO_2−Pd interfaces. The characterization results of g-Pd/SiO_2 suggested that preparing a well-dispersed Pd/SiO_2 is challenging even at low loading because the interaction between Pd and SiO_2 is not particularly strong.[31] In contrast to the case where larger-sized Pd particles had been formed prior to catalyst overcoating, the use of atomically dispersed $Pd(en)_2/SiO_2$ during catalyst preparation could minimize the loss of the external Pd surface occurring in the thermal reduction step.

https://dx.doi.org/10.1021/acscatal.0c02146
ACS Catal. 2020, 10, 12058−12070

In addition to SiO_2, the Pd complex can also be grafted on other metal oxide supports using the same procedure. We prepared $Pd(en)_2/ZrO_2$ and overcoated it with ZrO_2 to form ZrO_2@Pd/ZrO_2. This catalyst displayed a higher dispersion (70%, Table 1) than that of ZrO_2@Pd/SiO_2, which could be explained by the stronger interaction between Pd and the ZrO_2 support.[32] We also prepared a reference Pd/ZrO_2 using a standard wet impregnation method with the same Pd precursor and found that Pd was also highly dispersed (89%, Table 1). The slightly lower dispersion of the overcoated catalyst is likely due to coverage by the overcoat. Irreversible loss of active sites during overcoating is an issue that is challenging to solve.[11−13] Density functional theory (DFT) simulations have explained this coverage effect for ALD processes by showing that metal oxide precursors can interact with specific facets of nanoparticles.[33] Our past work showed that only 38% of Cu remained accessible after overcoating Cu/Al_2O_3 with analogous chelation chemistry-based sol−gel coating.[16] The overcoat formed using a nonhydrolytic sol−gel method even blocked up to 80% of the Pt sites of nanoparticles supported on SBA-15.[16] The smaller difference in dispersion between ZrO_2@Pd/ZrO_2 and Pd/ZrO_2 compared to the previous studies demonstrates again the advantage of using an atomically dispersed precatalyst as a starting material for catalyst engineering. We suggested that the high accessibility could be ascribed to not only the smaller particle size of ZrO_2@Pd/ZrO_2 but also the use of a precatalyst containing chelated Pd, which could have avoided the direct interaction between precursor and Pd atoms during the overcoating step.

Overcoat Effects on the Physical and Chemical Properties of the Catalysts. The physical and chemical properties of the overcoated and reference catalysts were further characterized. The N_2 physisorption isotherms showed that Al_2O_3@Pd/SiO_2 and ZrO_2@Pd/SiO_2 have nearly the same hysteresis loops as that of g-Pd/SiO_2 (Figure S4a). These three catalysts also had similar BET surface areas (with less than a 10% reduction after overcoating and sometimes a slight increase). These results were distinct from previous observations of ZrO_2-ALD processes where the overcoated catalysts showed reduced S_{BET} (from 100 to 66 m^2/g), which was indicative of a denser overcoat.[34] We analyzed ZrO_2@Pd/SiO_2 and found that the thickness of the ZrO_2 overlayer was roughly 1.5 nm (Figure S3b) after injecting 20 monolayer equivalents (defined by molecular projection of the precursor on the BET surface area of the catalyst) of the precursor.[17,24] The thickness of a ZrO_2 monolayer (0.075 nm) was greater than that of ZrO_2 prepared using ALD (0.02 nm/cycle).[34] Furthermore, ZrO_2@Pd/ZrO_2 showed approximately 20% larger surface area, and its hysteresis loop was slightly modified compared to the uncoated Pd/ZrO_2 (Figure S4b). All these results indicated that the sol−gel method produced a more porous metal oxide overcoat compared to gas-phase ALD, which was in agreement with our previous work.[17,24]

Several studies have shown that the chemical state of Pd (Pd/PdO ratio) was dependent on the metal oxide support, and this property could have important effects for certain catalytic applications.[34,35] In this work, we first used overcoating to create additional surface functionality on a catalyst with a relatively inert support (*e.g.*, SiO_2). X-ray photoelectron spectroscopy (XPS) was then performed to characterize the overcoated and reference catalysts. The deconvoluted spectra showed that 95% of Pd was in its metallic form (Figure 2a) when being supported on SiO_2. In comparison, Al_2O_3@Pd/SiO_2 had an increased atomic fraction of Pd(II) with a Pd(II)/Pd(0) ratio of 0.18, which was similar to that of Pd/Al_2O_3 (Figure 2b,c), indicating that the Al_2O_3 overcoat could form an Al_2O_3−Pd interface and thus alter the chemical state of the Pd nanoparticles. Deconvoluting XPS data for the catalysts containing ZrO_2 was more challenging because of the presence of two intense Zr 3p peaks in the same binding energy region.[36] The Pd signal was barely detectable on ZrO_2@Pd/SiO_2 (likely resulting from its lower metal loading) but could be observed on both ZrO_2@Pd/ZrO_2 and Pd/ZrO_2 (Figure 2d−f). The deconvolution models showed that ZrO_2@Pd/ZrO_2 had three times higher Pd(II)/Pd(0) ratio than that of uncoated Pd/ZrO_2. Given the relatively small size of the peaks of interest *versus* the intense Zr 3p signal, the consistency of the deconvolution models for these two catalysts was assessed by performing Monte Carlo (MC) simulations (details are described in the Supporting Information, Section 2.5). The distributions of Pd(II)/Pd(0) were obtained using the resulting simulated datasets (Figure S5). The median values for this ratio were 0.96 and 1.29 for Pd/ZrO_2 and ZrO_2@Pd/ZrO_2, respectively. In addition, the intervals of the distributions without the upper and lower 5% tails were [0.29,2.48] for Pd/ZrO_2 and [0.14,6.44] for ZrO_2@Pd/ZrO_2. Although the relatively high overlap between the distributions made the assessment less conclusive, the simulation result still suggested that ZrO_2 had a statistically significant effect on Pd and then increased its oxidation state. The fitting model and the analogy with the XPS conclusions for Al_2O_3@Pd/SiO_2 indirectly substantiated that a new ZrO_2−Pd interface was present on both ZrO_2@Pd/ZrO_2 and ZrO_2@Pd/SiO_2. We further hypothesized that the greater Pd(II)/Pd ratio of ZrO_2@Pd/ZrO_2 resulted from the smaller Pd size compared to Pd/ZrO_2 and the unique nanostructure of the overcoated catalyst. Compared to the usual Pd/metal oxide structure, the subnanometer Pd clusters embedded in the ZrO_2 and Al_2O_3 overcoats could have led to a stronger interaction between Pd and metal oxides, thus increasing the Pd(II) character. A similar trend was also observed when embedding single Pd atoms in a mesoporous alumina support.[37] The presented characterization results showed that designing heterogeneous catalysts using overcoating can not only produce unique inverted metal−support interfaces but also modify the chemical properties of nanoparticles.

CO_2 Hydrogenation Study. Many studies have concluded that metal−metal oxide interfaces play an important role during the catalytic conversion of CO_2.[38−40] Specifically, DFT simulations showed that these interfacial sites can facilitate the chemisorption of CO_2, which is the first step in the CO_2 conversion mechanism.[38,41] The importance of metal oxides and/or other promotors was also experimentally identified when studying CO_2 hydrogenation using Pd supported on activated carbon.[42] At atmospheric pressure, the activated (*i.e.*, chemisorbed) CO_2 intermediate could be subsequently converted into CO or/and CH_4 *via* reverse water-gas shift (RWGS) or/and methanation. Engineering metal−metal oxide interfaces using overcoating could represent a promising strategy to create these active interfacial sites while imparting improved thermal stability to materials used for CO_2 conversion. To test this hypothesis, CO_2 hydrogenation was run using a tubular quartz reactor heated at 450 °C and 1 atm. We chose a relatively high temperature in order to study the stability of Pd clusters under conditions favoring thermal sintering. g-Pd/SiO_2 showed a fairly high selectivity toward

https://dx.doi.org/10.1021/acscatal.0c02146
ACS Catal. 2020, 10, 12058−12070

CO (~80%, Table 2) but a very low conversion (approximately 2%, Figure S6), which was in agreement with previous work.[43] Selectivities toward CO and CH_4 for this control catalyst remained stable over 20 h time on stream. The low conversion of g-Pd/SiO_2 could be attributed to the slow activation of CO_2 on the relatively inert silica support. Using Pd supported on Al_2O_3 significantly increased the conversion (Figure 3a). Although the higher conversion could be partially ascribed to the higher dispersion of Pd/Al_2O_3, the rate of this catalyst was one order of magnitude higher than that of g-Pd/SiO_2, whereas Pd/Al_2O_3 was only about twice more dispersed. Dispersion thus cannot explain the lower reaction rate of g-Pd/SiO_2 alone. Instead, we attributed the increased rate to the formation of a Pd−Al_2O_3 interface that likely facilitated CO_2 activation. The result was in agreement with a previous study showing that Al_2O_3 and La_2O_3 could serve as a promotor for CO_2 activation.[42] Although Pd/Al_2O_3 had a higher activity, it was less selective toward CO (~60%, Table 2). According to Wang *et al.*, the selectivity of Pd/Al_2O_3 is highly dependent on the particle size of Pd and smaller Pd particles are more selective toward CO.[44] To study the effects of particle size and the Al_2O_3 overcoat on CO_2 hydrogenation, Al_2O_3@Pd/SiO_2 was tested, and it also showed a significantly higher rate (1.0 mmol $CO_2 \cdot g^{-1} \cdot Pd \cdot s^{-1}$, Table 2) compared to g-Pd/SiO_2 because of the formation of an Al_2O_3−Pd interface and smaller Pd clusters. Interestingly, the selectivity of Al_2O_3@Pd/SiO_2 was also improved. The initial measured CO selectivity reached 92%, and CH_4 selectivity was only 5% (Table 2). Although smaller Pd clusters tend to catalyze RWGS reaction and produce CO, selectivities above 90% have never been reported using Pd/Al_2O_3 even when Pd was nearly atomically dispersed.[42,44] However, we also observed that the yield of CO rapidly dropped with prolonged time on stream, (Figure 3b) while the conversion fluctuated between 5 and 10% and the CH_4 selectivity remained below 5% throughout the measurement. The reduced carbon balance indicated that this catalyst was likely catalyzing the formation of carbonaceous deposits. The formation of such carbon species is not uncommon during hydrocarbon conversion over acidic catalysts (*e.g.*, zeolites).[45] The Pd clusters located on the mixed Al_2O_3−SiO_2 interface appeared to have distinct catalytic properties from those of either Pd/Al_2O_3 or Pd/SiO_2. We assume that this Al_2O_3−SiO_2 interface forms acid sites and converted reaction intermediates into carbon deposits. NH_3-TPD also revealed that Al_2O_3@Pd/SiO_2 had more acid sites compared to uncoated Pd/Al_2O_3 (Figure S7). Consequently, even though some interesting properties and high initial CO selectivity were observed using Al_2O_3@Pd/SiO_2, the poor carbon balance over an extended period of time significantly limits its practical use.

In addition to Al_2O_3, ZrO_2 has also frequently been used to prepare catalysts, especially for producing methanol from CO_2.[46,47] Both theoretical calculations and *in situ* experiments have shown that CO_2 can chemisorb and then be activated on the ZrO_2 surface.[48] For this reason, we prepared and tested another series of catalysts with ZrO_2, which was used both as a support and overcoat. Similar to Al_2O_3@Pd/SiO_2, the activity was significantly improved after overcoating ZrO_2 on Pd/SiO_2, confirming the high activity of Pd−ZrO_2 interfaces for catalyzing CO_2 reduction (Figure 4a). More importantly, ZrO_2@Pd/SiO_2 outperformed any catalysts containing Al_2O_3. Because Pd/Al_2O_3, Al_2O_3@Pd/SiO_2, and ZrO_2@Pd/SiO_2 have similar dispersions and loadings (Table 1), we concluded that the Pd−ZrO_2 interface is more active for catalytic CO_2 activation than the Pd−Al_2O_3 interface. Moreover, the use of ZrO_2@Pd/SiO_2 not only led to a high CO selectivity (~80%, Table 2) but also showed little deactivation. Unlike Al_2O_3@Pd/SiO_2 that led to pronounced carbon deposition over time, ZrO_2@Pd/SiO_2 maintained a carbon balance over 95% (Table 2) and CH_4 selectivity slightly decreased during the reaction (Figure S8a). Because the comparison of catalytic results of Al_2O_3@Pd/SiO_2 and Pd/Al_2O_3 indicated that distinct catalytic properties could appear when a mixed oxide interface was introduced, we subsequently studied Pd/ZrO_2 to see whether this reference catalyst showed substantially different catalytic

Table 2. Summary of CO_2 Hydrogenation Results of the Reference and Overcoated Catalysts

	($mmol\ CO_2 \cdot g^{-1} \cdot Pd \cdot s^{-1}$)		observed selectivity (%)		selectivity at 20 h (%)	
catalyst	observed rate[a]	rate at 20 h	CO	CH_4	CO	CH_4
g-Pd/SiO_2	0.16	0.14	79	21	83	17
ZrO_2@Pd/SiO_2	3.9	2.9	79	22	87	12
Al_2O_3@Pd/SiO_2	1.0	1.0	92	5	23	0
ZrO_2@Pd/ZrO_2	3.6	2.0	91	9	100	0
Pd/Al_2O_3	2.3	1.8	60	44	56	43
Pd/ZrO_2	4.5	2.2	77	23	92	6

[a]Calculated using the conversion before deactivation (0 h time on stream). The calculated rates and selectivities were based on the data shown by the solid line in Figures 3 and 4. For the most active series of catalysts (containing ZrO_2), all the relevant conversions were within the range between 30 and 40%. Because the active site (metal−metal oxide interface) for CO_2 hydrogenation is difficult to precisely define and probe, the rate was normalized by the total number of Pd atoms.

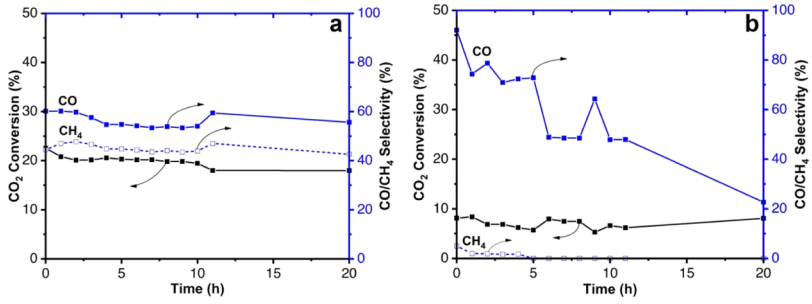

Figure 3. Conversion, CO selectivity, and CH_4 selectivity during CO_2 hydrogenation over (a) Pd/Al_2O_3 and (b) Al_2O_3@Pd/SiO_2. The details of the reaction condition are described in the Supporting Information.

https://dx.doi.org/10.1021/acscatal.0c02146
ACS Catal. 2020, 10, 12058−12070

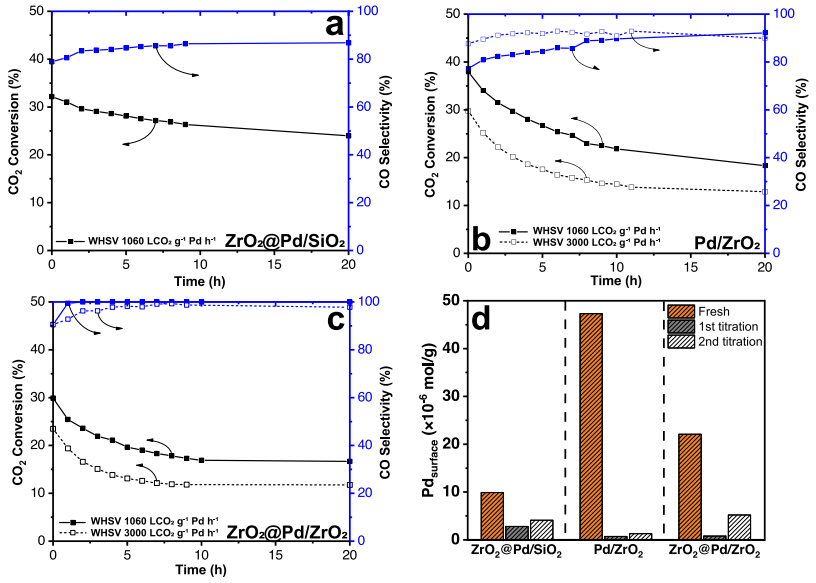

Figure 4. CO_2 hydrogenation catalyzed by (a) ZrO_2@Pd/SiO_2, (b) Pd/ZrO_2, and (c) ZrO_2@Pd/ZrO_2. To be able to compare the conversions directly, the mass of the catalyst in the reactor was adjusted so as to obtain the same WHSV (1060 $LCO_2 \cdot g^{-1} \cdot Pd \cdot h^{-1}$ for solid lines and 3000 $LCO_2 \cdot g^{-1} \cdot Pd \cdot h^{-1}$ for dash lines) (d) CO chemisorption measurements of the fresh and spent catalysts (targeting total and reversible deactivations by first and second titrations, respectively).

properties. To facilitate the comparison of the activities, the weight of Pd/ZrO_2 in the reactor was adjusted (to 30 mg) based on its loading in order to have the same weight hourly space velocity (WHSV, based on total Pd). Using Pd/ZrO_2 led to a higher conversion (Figure 4b), presumably because the Pd was better dispersed (89%, Table 1). This catalyst also had a similarly high CO selectivity (77%, Table 2). Interestingly, the selectivity towards CO increased over time (to 92% at 20 h), while CH_4 selectivity decreased (Figure S8b). Although the use of Pd/ZrO_2 led to a slightly higher conversion and CO selectivity compared to the use of ZrO_2@Pd/SiO_2, Pd/ZrO_2 deactivated faster than the overcoated catalyst.

Water is a product in RWGS, and the presence of steam has been identified as a factor that accelerates catalyst deactivation.[49] Furthermore, the reaction temperature (450 °C) was close to the Hüttig temperature of Pd (548 °C) (*i.e.*, the temperature at which the mobility of surface atoms increases substantially) and above the Hüttig temperature of PdO (307 °C).[50] Under these harsh operating conditions, the undercoordinated Pd atom is likely quite mobile. In gas-phase reactions, particle growth can result from both particle coalescence and Ostwald ripening.[51] A recent microscopy study has shown that the undercoordinated Pd atoms on the particle surface possess high surface energy and are mobile.[52] Our XPS results indicated that the overcoats can interact with Pd to the extent that an increased Pd(II) character was suggested. Therefore, we speculate that the ZrO_2 overcoat may have reduced the mobility of undercoordinated Pd atoms, thus reducing particle sintering. This effect had been previously observed when overcoating a Cu catalyst with Al_2O_3.[53] Moreover, ZrO_2 could also serve as a physical barrier that results in a longer pathway for the migrating particle to reach another particle, which delays coalescence.

Finally, ZrO_2@Pd/ZrO_2 was also tested to investigate the effects of the overcoat when Pd was supported on ZrO_2. At identical WHSVs, the conversion over ZrO_2@Pd/ZrO_2 was close to that of ZrO_2@Pd/SiO_2 but still lower than that of Pd/ZrO_2. Although the observed rates (normalized with respect to total Pd) of ZrO_2@Pd/ZrO_2 and ZrO_2@Pd/SiO_2 were similar (Table 2), we also found that ZrO_2@Pd/ZrO_2 and Pd/ZrO_2 had nearly the same activity, when considering accessible surface Pd as measured by CO chemisorption (~5.1 $CO_2 \cdot g^{-1} \cdot Pd_{surface} \cdot s^{-1}$). Interestingly, ZrO_2@Pd/SiO_2 had the highest rate after applying such a normalization (~10.3 $CO_2 \cdot g^{-1} \cdot Pd_{surface} \cdot s^{-1}$). These results suggested that the energy barrier of the rate-determining step might be the lowest when Pd was supported on a SiO_2−ZrO_2 mixture. However, because $Pd_{surface}$ measured by CO adsorption does not necessarily represent the active site of the rate-determining step (which was hypothesized to be Pd−metal oxide interfaces), whether supporting Pd on a SiO_2−ZrO_2 is particularly favorable for converting CO_2 will require further investigation. Even though the initial conversion of ZrO_2@Pd/ZrO_2 was the lowest among the catalysts containing ZrO_2, the CO selectivity of ZrO_2@Pd/ZrO_2 was the highest (91%, Table 2), and it quickly increased to 100% within 2 h (Figure 4c). No CH_4 was detected from 2 to 20 h time on stream (Figure S8c). Among several metals that catalyze CO_2 hydrogenation, Cu-based catalysts have been reported to have a selectivity of 100% toward CO at atmospheric pressure because they had very little activity for methanation.[54,55] However, compared to Cu, noble metals such as Pd usually have a higher rate for CO_2 conversion. For instance, at atmospheric pressure, the rate of Cu/ZnO/Al_2O_3 (a benchmark catalyst used in industry that can also be employed to produce methanol at more elevated pressures) at 600 °C was reported as 1.2 mmol $CO_2 \cdot g^{-1} \cdot Cu \cdot s^{-1}$ with 100% CO selectivity, whereas the rate for the reference Pd/Al_2O_3 catalyst we measured here reached 2.3 mmol $CO_2 \cdot g^{-1} \cdot Pd \cdot s^{-1}$ at 450 °C.[55] Nevertheless, noble metals typically also catalyze methanation, which decreases CO selectivity. Importantly, ZrO_2@Pd/ZrO_2 could not only selectively convert CO_2 to CO but also outperform the benchmark Cu/ZnO/Al_2O_3 in terms of the CO_2 conversion rate (with a stable value of 2 mmol $CO_2 \cdot g^{-1} \cdot Pd \cdot s^{-1}$ after 10 h time on stream at 450 °C). Attempts to inhibit the competing methanation over supported noble metal catalysts have been made, notably by

https://dx.doi.org/10.1021/acscatal.0c02146
ACS Catal. 2020, 10, 12058−12070

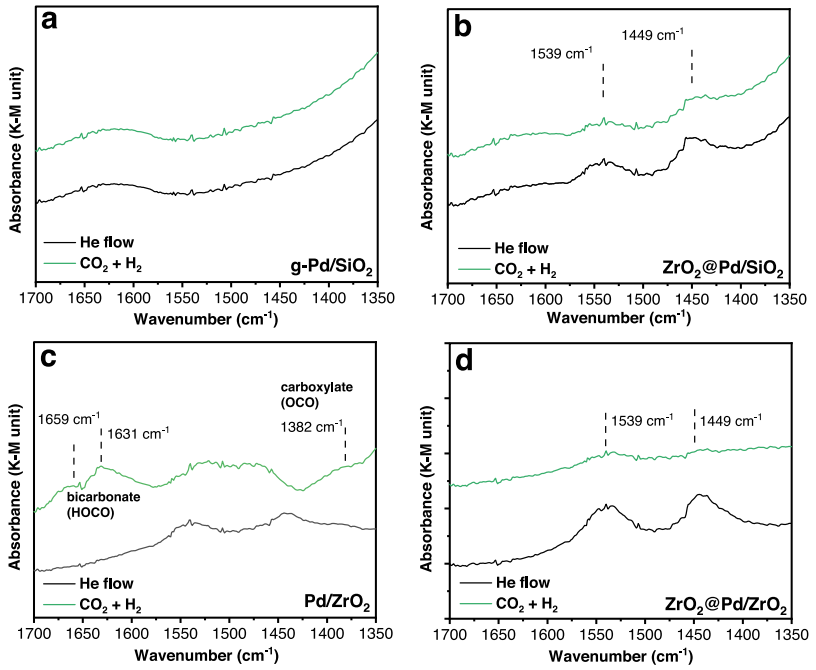

Figure 5. *In situ* DRIFTS spectra in Kubelka–Munk (K–M) transformation units measured in the presence of He and then CO_2 and H_2 for (a) g-Pd/SiO_2, (b) ZrO_2@Pd/SiO_2, (c) Pd/ZrO_2, and (d) ZrO_2@Pd/ZrO_2.

controlling particle size and the porous environment.[42,56−59] However, to the best of our knowledge, this is the first Pd-based catalyst to reach 100% CO selectivity. To demonstrate that Pd/ZrO_2 cannot reach 100% selectivity toward CO at the same conversion, we reduced the weight of Pd/ZrO_2 (to 10 mg) to have the same conversion as the overcoated catalyst (dash line in Figure 4b). The resulting CO selectivity slightly increased but fluctuated at around 90% throughout the test. Although this result emphasized the unique catalytic property of the ZrO_2@Pd/ZrO_2 material, it also indicated that the selectivity was dependent on conversion. Therefore, we similarly varied the conversion of ZrO_2@Pd/ZrO_2 by reducing the catalyst's weight (to 17 mg) in the reactor. The initial CO selectivity of ZrO_2@Pd/ZrO_2 remained the same (around 90%) at 24% conversion and once again increased to nearly 100% with additional time on stream. Moreover, similar to what we have observed when studying ZrO_2@Pd/SiO_2, ZrO_2@Pd/ZrO_2 also deactivated more slowly compared to Pd/ZrO_2. ZrO_2@Pd/ZrO_2 did deactivate in the early stage but the conversion remained relatively stable after 10 h. In contrast, Pd/ZrO_2 continuously deactivated throughout the catalytic run. Based on these results, we concluded that not only could the ZrO_2 overcoat engineer a new ZrO_2–Pd interface and result in an exceptional CO selectivity but it could also mitigate deactivation under harsh reaction conditions (450 °C in the presence of steam).

Deactivation Study of Catalysts. To study the deactivation mechanism, CO_2 hydrogenation was run using ZrO_2@Pd/SiO_2, Pd@ZrO_2, and ZrO_2@Pd/ZrO_2 on a Micromeritics Autochem, which allows us to perform CO chemisorption directly on spent catalysts. The reaction was run for 48 h, reduced again at 300 °C with a flow of H_2, after which the spent catalysts were titrated using CO pulses. To verify whether carbon deposition occurred (which causes reversible deactivation), a subsequent second CO chemisorption measurement was performed after calcining the spent catalysts for 1 h followed by reduction. The first CO titration showed that the $Pd_{surface}$ on the three spent catalysts was reduced after 48 h of reaction. The first CO titration showed that the spent ZrO_2@Pd/SiO_2 had the most $Pd_{surface}$ sites and the spent Pd/ZrO_2 had the least $Pd_{surface}$ sites (Figure 4d), which agreed with the observed trend of deactivation rates in the catalysis tests (Figure 4a–c). Interestingly, all spent catalysts showed increased $Pd_{surface}$ after calcination, which suggested the presence of carbonaceous deposits on the spent catalysts. After removing the deposits by calcination, Pd/ZrO_2 still lost the largest amount of $Pd_{surface}$ (from 47.3 to 1.2 μmol). Large agglomerated Pd particles were also observed when analyzing the spent Pd/ZrO_2 by STEM (Figure S9). These results confirmed that the catalysts with a ZrO_2 overcoat were more sintering-resistant under harsh reaction conditions. Among the three spent catalysts, the ZrO_2@Pd/ZrO_2 catalyst recovered the most $Pd_{surface}$ (from 0.8 to 5 μmol) after calcination. In contrast, calcination had more limited effects on Pd/ZrO_2 and ZrO_2@Pd/SiO_2, which suggested that more carbonaceous deposits formed on ZrO_2@Pd/ZrO_2. Based on the deactivation study, we concluded that catalyst deactivation was caused by both sintering and carbon deposition. The larger amount of deposits formed over ZrO_2@Pd/ZrO_2 was particularly interesting, given that the increase in CO selectivity accompanied the initial deactivation (the deactivation slowed down after CO selectivity reached 100%). This selectivity change was unlikely caused by particle sintering because a past work has shown that smaller Pd particles are more selective toward CO when catalyzing RWGS reaction.[44] Additionally, if Pd nanoparticles with a specific size could lead to 100% CO selectivity, the same phenomenon would have been observed on Pd/ZrO_2 once the Pd agglomerates had formed. The increase in selectivity toward CO because of dynamic changes of catalysts during CO_2 hydrogenation has been previously reported including self-poisoning on Ru/CeO_2 and the transformation of methanation sites on Rh/TiO_2.[56,60] Specifically, the switch from methanation to RWGS sites on Rh/TiO_2 was induced by the encapsulation of Rh by a thin

https://dx.doi.org/10.1021/acscatal.0c02146
ACS Catal. 2020, 10, 12058−12070

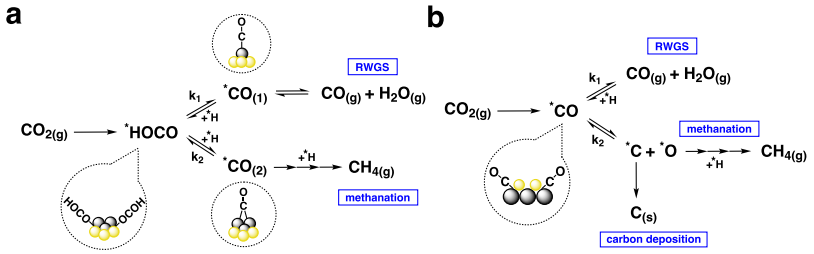

Figure 6. Proposed reaction networks of (a) Pd/ZrO_2 and (b) ZrO_2@Pd/ZrO_2. The yellow and gray spheres represent ZrO_2 and Pd, respectively.

reducible metal oxide overcoat *via* strong metal support interaction.[60] Because ZrO_2 is a nonreducible metal oxide and Pd had been overcoated, active-site transformation was unlikely. Therefore, we propose that the superior CO selectivity of ZrO_2@Pd/ZrO_2 resulted from the selective carbon deposition on its methanation sites.

***In Situ* DRIFTS Characterization and Reaction Mechanism.** To better understand the higher selectivity of ZrO_2@Pd/ZrO_2 toward CO and the reaction mechanism, *in situ* DRIFTS measurements were carried out to identify the reaction intermediates. The catalysts were reduced with a flow of H_2 at 300 °C, and then, the feed was switched to He. Subsequently, the temperature was elevated to 450 °C, and the first spectrum was measured (black line in Figure 5). The feed was then switched to a mixture of CO_2 and H_2, and the second spectrum was recorded (green line in Figure 5). ZrO_2@Pd/SiO_2, ZrO_2@Pd/ZrO_2, and Pd/ZrO_2 displayed similar spectra before beginning the flow of CO_2 and H_2. The two small bands at 1539 and 1449 cm^{-1} were assigned to the strongly bound H_2O.[61,62] These two bands were not observed on g-Pd/SiO_2, suggesting that most of the physisorbed water had been removed during reduction, which was likely because of the weaker interaction between SiO_2 and H_2O. Surprisingly, only Pd@ZrO_2 showed new absorbance bands, whereas g-Pd/SiO_2, ZrO_2@Pd/SiO_2, and ZrO_2@Pd/ZrO_2 displayed similar spectra under reaction conditions as they did in the presence of only He. By analogy with past reports, the bands that were only observed under reaction conditions for Pd/ZrO_2 were assigned to bicarbonate-derived species.[44,63,64] Therefore, we concluded that CO_2 was converted *via* the bicarbonate-mediated RWGS pathway on Pd/ZrO_2. In contrast, the other three catalysts might activate CO_2 through the direct C−O cleavage pathway because no absorbance associated with either formate or bicarbonate was observed.[57,65] The intensity of the water bands decreased when CO_2 and H_2 were present. Strongly bound water can be found on the zirconium center that has oxygen vacancies and is more electrophilic.[61] The desorption of water might result from the competitive chemisorbed CO_2, and this observation is consistent with a hypothesis suggesting that oxygen vacancy is critical for CO_2 activation.[66]

The bicarbonate-mediated mechanism on Pd/ZrO_2 is similar to a reported mechanism on an analogous Pd/Al_2O_3 system (Figure 6a).[44] The first step is the chemisorption of CO_2, presumably on the zirconium center with O vacancies according to our DRIFTS measurements. The chemisorbed CO_2 then either interacted with surface hydroxyl groups or dissociated H to form bicarbonate-like intermediates. According to Wang *et al.*,[44] these intermediates could be further converted to the adsorbed CO intermediate that can be either bound with an isolated Pd atom linearly (k_1) or with Pd atoms with twofold or threefold coordination (k_2). CO configuration is known to be particularly influential on CO and CH_4 selectivities.[44,58] The linearly adsorbed CO has a lower desorption barrier, thus eventually forming the CO product, whereas the twofold and threefold coordinated CO are more susceptible to further hydrogenation into CH_4. Therefore, several groups have proposed that methanation and RWGS occur on two different sites and reducing the nanoparticles' size can favor the production of CO because it creates a larger fraction of isolated metal sites that bond CO with linear configuration.[44,56,57] Although chemisorbed CO was not observed during *in situ* DRIFTS measurements (likely because of the short lifetime of CO intermediates at high temperature), we performed CO chemisorption on Pd/ZrO_2 at room temperature, and the signal of linearly bound CO was detected by DRIFTS (Figure S10a). Because of the high dispersion of Pd on ZrO_2, many isolated Pd atoms or small clusters sites were likely present on the surface, which favored the production of CO (above 80% selectivity).[58] Besides linearly bound CO, twofold and threefold coordinated CO species were also observed, indicating the presence of bigger particles that catalyzed methanation.[58] Because the RWGS reaction and methanation are governed by two different active sites, the aforementioned increased CH_4 selectivity at higher conversion can be explained by the competing RWGS and methanation reactions. The equilibrium conversion of RWGS under our condition was calculated as 43%.[67] Therefore, the production of CO was close to the thermodynamic equilibrium in our first run at higher conversion (solid line, Figure 4b). Under such conditions, any excess amount of catalyst would not produce more CO but just contribute to methanation. Once Pd/ZrO_2 deactivated, the RWGS reaction was no longer close to the thermodynamic equilibrium, which allowed the active sites to increase the net rates of RWGS compared to methanation and then increased CO selectivity to 90% (similar to that obtained at lower conversion, dashed line, Figure 4b).

As previously mentioned, we did not observe any absorbances representing formate and bicarbonate intermediates when running *in situ* DRIFTS measurements on the catalysts with ZrO_2 overcoat (Figure 5b,d). In the absence of these intermediates and because there are only three known mechanisms of CO_2 hydrogenation (bicarbonate mediated, formate mediated, or the direct C−O cleavage pathway), we hypothesized that CO_2 was likely converted through the C−O cleavage route on ZrO_2@Pd/ZrO_2 and ZrO_2@Pd/SiO_2. Our XPS data showed an increased Pd(II) character in ZrO_2@Pd/ZrO_2, implying the formation of a new type of interfacial site (*i.e.*, the active site for CO_2 activation) with distinct chemical properties, which led to a different catalytic performance. Because the modification of the active site may result from the distinct chemistry of the ZrO_2 overcoat synthesized through the sol−gel route, we further performed powder X-ray diffraction to characterize the overcoated and reference catalysts, and the results showed that our ZrO_2 overcoat is

https://dx.doi.org/10.1021/acscatal.0c02146
ACS Catal. 2020, 10, 12058−12070

amorphous, whereas the commercial ZrO_2 support has a monoclinic structure (Figure S11). Accordingly, we attributed the switch of reaction pathways to the presence of this newly engineered interfacial site comprising an amorphous ZrO_2 overcoat, which is different from the interface present on Pd over monoclinic ZrO_2. On this ZrO_2 (amorphous)−Pd interface, CO_2 could initially chemisorb on O vacancies, which is similar to the bicarbonate-mediated pathway but follows a different mechanism in the next step. According to the DFT simulation of the C−O cleavage pathway, the dissociation of the first C−O bond was followed by the formation of water (the other product of RWGS reaction), which involved the reaction of dissociated *O (from CO_2) and *H (from H_2, adsorbed on Pd).[38,57] Therefore, CO_2 cleavage might occur on the ZrO_2−Pd interface, and then, a CO intermediate was formed (Figure 6b). The DFT study also suggested that the adsorbed CO can either desorb (k_1) or further dissociate (k_2).[57] Accordingly, the energy barriers of CO dissociation and desorption are two key factors controlling CO and CH_4 selectivities. CO-DRIFTS characterization of ZrO_2@Pd/ZrO_2 showed that CO could chemisorb on the surface in both linear and bridge configurations (Figure S10b). Similar to what was reported for the bicarbonate-mediated pathway, the different configurations of CO could have led to different energy barriers for C−O cleavage, which governed the final CO/CH_4 selectivity. Importantly, DFT simulation showed that the formation of CH_4 in the C−O cleavage pathway requires a second C−O cleavage of the CO intermediate, forming *C and *O.[57] Based on our CO deactivation studies of spent catalysts (Figure 4d), we hypothesized that the adsorbed *C could not only be hydrogenated to CH_4 but also nucleate on the surface and form carbonaceous deposits. This hypothesis could explain the self-poisoning phenomenon observed by Aitbekova *et al.* and us.[56] On the ZrO_2@Pd/ZrO_2, a small fraction of the CO intermediate that adsorbed on the sites favoring further C−O cleavage was initially converted into CH_4 (at 10% selectivity in our initial measurement). However, carbon deposition likely occurred on the same active sites, which quickly limited methanation (causing the fast initial deactivation), and subsequently, the selectivity toward CO increased to 100%. Interestingly, the monoclinic ZrO_2 support seemed to play an important role in this phenomenon because this self-poisoning effect was less discernible when using ZrO_2@Pd/SiO_2 (its CO selectivity only slightly increased and the calcination treatment led to a smaller recovery of $Pd_{surface}$). Because a mixed oxide interface might influence this poisoning effect, as an extra control, we synthesized an amorphous ZrO_2 support by depositing ZrO_2 onto SiO_2 (ZrO_2@SiO_2) and then used it to prepare Pd/ZrO_2@SiO_2 (which can be used to mostly probe the effect of a Pd−amorphous ZrO_2 interface) and use it for CO_2 hydrogenation (Figure S12). Although *in situ* DRIFTS (Figure S13) indicated that Pd/ZrO_2@SiO_2 also converted CO_2 through the direct C−O cleavage pathway, its selectivity toward CO was slightly decreased with extended time on stream. The catalysis results of Pd/ZrO_2 ZrO_2@Pd/SiO_2 and Pd/ZrO_2@SiO_2 underlined the importance of ZrO_2@Pd/ZrO_2's structure. The exceptional CO selectivity could only be achieved when Pd was simultaneously in contact with both monoclinic and amorphous ZrO_2. The interesting catalytic behavior of ZrO_2@Pd/ZrO_2 could be explained by the sensitivity of sub-nanometer metal clusters to their local coordination environment (which was contributed by both the ZrO_2 overcoat and support).[68] As a result, Pd clusters coordinated with two ZrO_2 polymorphs could have led to a unique reactivity that facilitated selective carbon deposition. Further elucidation of the factors governing the self-poisoning of methanation sites would require further theoretical and analytical investigations including DFT simulations and more advanced *in situ* spectroscopies.

CONCLUSIONS

A sol−gel-based synthetic approach was developed to prepare an atomically dispersed Pd(en)$_2$/SiO_2 that served as a precatalyst and was subsequently used in a synthesis procedure featuring kinetically controlled sol−gel overcoating. Overcoating this atomically dispersed material with metal oxides prior to reduction led to a final catalyst containing metal oxide−Pd interface sites with high dispersion. In contrast to the traditional method where Pd particles had been formed on SiO_2 prior to coating, this new synthetic approach could limit particle growth during thermal activation, resulting in highly accessible sub-nanometer Pd clusters. Because of the formation of new metal oxide−metal interfaces, both ZrO_2@Pd/SiO_2 and Al_2O_3@Pd/SiO_2 showed significantly improved activity for CO_2 hydrogenation compared to the uncoated g-Pd/SiO_2. Moreover, this strategy could be applied to additional metal oxide supports to synthesize catalysts with distinct catalytic properties. Specifically, when using Pd(en)$_2$/ZrO_2 to synthesize a ZrO_2@Pd/ZrO_2 catalyst, the overcoat not only mitigated the agglomeration of Pd under the severe reaction condition but also increased the CO selectivity. This improvement of selectivity was attributed to the self-poisoning of the methanation sites by carbon deposition, which was only favored on the ZrO_2@Pd/ZrO_2 catalyst, leading to an unprecedented 100% CO selectivity on Pd after 1 h time on stream. The partially deactivated ZrO_2@Pd/ZrO_2 then maintained a stable reaction rate with prolonged time on stream. These results demonstrate the potential of overcoated supported noble metals in CO_2 reduction to CO, especially considering their superior activity, selectivity, and thermal stability.

ASSOCIATED CONTENT

Supporting Information

The Supporting Information is available free of charge at https://pubs.acs.org/doi/10.1021/acscatal.0c02146.

Additional characterization data and experimental details including catalyst synthesis, characterizations, and CO_2 hydrogenation study (PDF)

AUTHOR INFORMATION

Corresponding Author

Jeremy S. Luterbacher − *Institute of Chemical Sciences and Engineering, École Polytechnique Fédérale de Lausanne (EPFL), 1015 Lausanne, Switzerland;* orcid.org/0000-0002-0967-0583; Email: jeremy.luterbacher@epfl.ch

Authors

Yuan-Peng Du − *Institute of Chemical Sciences and Engineering, École Polytechnique Fédérale de Lausanne (EPFL), 1015 Lausanne, Switzerland;* orcid.org/0000-0002-4329-4008

Ali M. Bahmanpour − *Institute of Chemical Sciences and Engineering, École Polytechnique Fédérale de Lausanne (EPFL),*

1015 Lausanne, Switzerland; orcid.org/0000-0003-2092-9215

Luka Milošević − *Institute of Chemical Sciences and Engineering, École Polytechnique Fédérale de Lausanne (EPFL), 1015 Lausanne, Switzerland*

Florent Héroguel − *Institute of Chemical Sciences and Engineering, École Polytechnique Fédérale de Lausanne (EPFL), 1015 Lausanne, Switzerland;* orcid.org/0000-0003-2210-7119

Mounir D. Mensi − *Institute of Chemical Sciences and Engineering, École Polytechnique Fédérale de Lausanne (EPFL), 1015 Lausanne, Switzerland*

Oliver Kröcher − *Institute of Chemical Sciences and Engineering, École Polytechnique Fédérale de Lausanne (EPFL), 1015 Lausanne, Switzerland; Bioenergy and Catalysis Laboratory, Paul Scherrer Institute, 5232 Villigen PSI, Switzerland;* orcid.org/0000-0002-7268-7257

Complete contact information is available at: https://pubs.acs.org/10.1021/acscatal.0c02146

Notes

The authors declare no competing financial interest.

■ ACKNOWLEDGMENTS

This work was supported by the European Research Council (ERC) under the European Union's Horizon 2020 research and innovation program (starting grant: CATACOAT, no 758653), the Swiss National Science Foundation through grant PYAPP2_154281, and EPFL. This work was also accomplished within the framework of the Swiss Competence Center for Bioenergy Research (SCCER-BIOSWEET). We thank Tzu-Hsien Shen for the help during electron microscopy measurements. We also thank Dr. Natalia Gasilova for her help in performing measurements with ICP-OES.

■ REFERENCES

(1) Nørskov, J. K.; Studt, F.; Abild-Pedersen, F.; Bligaard, T. *Fundamental Concepts in Heterogeneous Catalysis*, 1 ed.; Wiley: Hoboken, New Jersey, 2014.

(2) Liu, Y.; Liu, J.; Feng, G.; Yin, S.; Cen, W.; Liu, Y. Interface effects for the hydrogenation of CO2 on Pt4/γ-Al2O3. *Appl. Surf. Sci.* **2016**, *386*, 196−201.

(3) Lam, E.; Corral-Pérez, J. J.; Larmier, K.; Noh, G.; Wolf, P.; Comas-Vives, A.; Urakawa, A.; Copéret, C. CO 2 Hydrogenation on Cu/Al 2 O 3 : Role of the Metal/Support Interface in Driving Activity and Selectivity of a Bifunctional Catalyst. *Angew. Chem., Int. Ed.* **2019**, *58*, 13989−13996.

(4) Carrasquillo-Flores, R.; Ro, I.; Kumbhalkar, M. D.; Burt, S.; Carrero, C. A.; Alba-Rubio, A. C.; Miller, J. T.; Hermans, I.; Huber, G. W.; Dumesic, J. A. Reverse Water-Gas Shift on Interfacial Sites Formed by Deposition of Oxidized Molybdenum Moieties onto Gold Nanoparticles. *J. Am. Chem. Soc.* **2015**, *137*, 10317−10325.

(5) Ro, I.; Resasco, J.; Christopher, P. Approaches for Understanding and Controlling Interfacial Effects in Oxide-Supported Metal Catalysts. *ACS Catal.* **2018**, *8*, 7368−7387.

(6) Liu, X.; Zhu, Q.; Lang, Y.; Cao, K.; Chu, S.; Shan, B.; Chen, R. Oxide-Nanotrap-Anchored Platinum Nanoparticles with High Activity and Sintering Resistance by Area-Selective Atomic Layer Deposition. *Angew. Chem.* **2017**, *129*, 1670−1674.

(7) Lu, J.; Fu, B.; Kung, M. C.; Xiao, G.; Elam, J. W.; Kung, H. H.; Stair, P. C. Coking- and Sintering-Resistant Palladium Catalysts Achieved Through Atomic Layer Deposition. *Science* **2012**, *335*, 1205−1208.

(8) Zhang, J.; Wang, B.; Nikolla, E.; Medlin, J. W. Directing Reaction Pathways through Controlled Reactant Binding at Pd-TiO2 Interfaces. *Angew. Chem., Int. Ed.* **2017**, *56*, 6594−6598.

(9) Zhao, G.; Yang, F.; Chen, Z.; Liu, Q.; Ji, Y.; Zhang, Y.; Niu, Z.; Mao, J.; Bao, X.; Hu, P.; Li, Y. Metal/Oxide Interfacial Effects on the Selective Oxidation of Primary Alcohols. *Nat. Commun.* **2017**, *8*, 14039.

(10) Zhang, J.; Medlin, J. W. Catalyst Design Using an Inverse Strategy: From Mechanistic Studies on Inverted Model Catalysts to Applications of Oxide-Coated Metal Nanoparticles. *Surf. Sci. Rep.* **2018**, *73*, 117−152.

(11) Zhang, H.; Gu, X.-K.; Canlas, C.; Kropf, A. J.; Aich, P.; Greeley, J. P.; Elam, J. W.; Meyers, R. J.; Dumesic, J. A.; Stair, P. C.; Marshall, C. L. Atomic Layer Deposition Overcoating: Tuning Catalyst Selectivity for Biomass Conversion. *Angew. Chem., Int. Ed.* **2014**, *53*, 12132−12136.

(12) Weng, Z.; Zaera, F. Sub-Monolayer Control of Mixed-Oxide Support Composition in Catalysts via Atomic Layer Deposition: Selective Hydrogenation of Cinnamaldehyde Promoted by (SiO2-ALD)-Pt/Al2O3. *ACS Catal.* **2018**, *8*, 8513−8524.

(13) Liang, H.; Zhang, B.; Ge, H.; Gu, X.; Zhang, S.; Qin, Y. Porous TiO2/Pt/TiO2 Sandwich Catalyst for Highly Selective Semihydrogenation of Alkyne to Olefin. *ACS Catal.* **2017**, *7*, 6567−6572.

(14) O'Neill, B. J.; Jackson, D. H. K.; Lee, J.; Canlas, C.; Stair, P. C.; Marshall, C. L.; Elam, J. W.; Kuech, T. F.; Dumesic, J. A.; Huber, G. W. Catalyst Design with Atomic Layer Deposition. *ACS Catal.* **2015**, *5*, 1804−1825.

(15) Monnier, B. P. L.; Wells, F.; Talebkeikhah, F.; Luterbacher, J. S. Atomic Layer Deposition on Dispersed Materials in Liquid Phase by Stoichiometrically Limited Injections. *Adv. Mater.* **2019**, *31*, 1904276.

(16) Du, Y.-P.; Héroguel, F.; Luterbacher, J. S. Slowing the Kinetics of Alumina Sol-Gel Chemistry for Controlled Catalyst Overcoating and Improved Catalyst Stability and Selectivity. *Small* **2018**, *14*, 1801733.

(17) Héroguel, F.; Silvioli, L.; Du, Y.-P.; Luterbacher, J. S. Controlled Deposition of Titanium Oxide Overcoats by Non-Hydrolytic Sol Gel for Improved Catalyst Selectivity and Stability. *J. Catal.* **2018**, *358*, 50−61.

(18) Du, Y.-P.; Héroguel, F.; Nguyen, X. T.; Luterbacher, J. S. Post-synthesis deposition of mesoporous niobic acid with improved thermal stability by kinetically controlled sol-gel overcoating. *J. Mater. Chem. A* **2019**, *7*, 23803−23811.

(19) Lu, J.; Stair, P. C. Low-Temperature ABC-Type Atomic Layer Deposition: Synthesis of Highly Uniform Ultrafine Supported Metal Nanoparticles. *Angew. Chem., Int. Ed.* **2010**, *49*, 2547−2551.

(20) Fujita, M.; Yazaki, J.; Ogura, K. Preparation of a macrocyclic polynuclear complex, [(en)Pd(4,4′-bpy)]4(NO3)8 (en = ethylenediamine, bpy = bipyridine), which recognizes an organic molecule in aqueous media. *J. Am. Chem. Soc.* **1990**, *112*, 5645−5647.

(21) Ro, I.; Xu, M.; Graham, G. W.; Pan, X.; Christopher, P. Synthesis of Heteroatom Rh-ReOx Atomically Dispersed Species on Al2O3 and Their Tunable Catalytic Reactivity in Ethylene Hydroformylation. *ACS Catal.* **2019**, *9*, 10899−10912.

(22) Schubert, U.; Huesing, N.; Lorenz, A. Hybrid Inorganic-Organic Materials by Sol-Gel Processing of Organofunctional Metal Alkoxides. *Chem. Mater.* **1995**, *7*, 2010−2027.

(23) Chiang, Y.-D.; Dutta, S.; Chen, C.-T.; Huang, Y.-T.; Lin, K.-S.; Wu, J. C. S.; Suzuki, N.; Yamauchi, Y.; Wu, K. C.-W. Functionalized Fe3O4@Silica Core-Shell Nanoparticles as Microalgae Harvester and Catalyst for Biodiesel Production. *ChemSusChem* **2015**, *8*, 789−794.

(24) Du, Y.-P.; Héroguel, F.; Nguyen, X. T.; Luterbacher, J. S. Post-synthesis deposition of mesoporous niobic acid with improved thermal stability by kinetically controlled sol-gel overcoating. *J. Mater. Chem. A* **2019**, *7*, 23803.

(25) Yamada, K.; Chow, T. Y.; Horihata, T.; Nagata, M. A Low Temperature Synthesis of Zirconium Oxide Coating Using Chelating Agents. *J. Non-Cryst. Solids* **1988**, *100*, 316−320.

(26) Soled, S. Case Studies of Nobel-Metal Catalysts. *Synthesis of Solid Catalysts*; John Wiley & Sons, Ltd, 2009; pp 353−367.

(27) Ding, K.; Cullen, D. A.; Zhang, L.; Cao, Z.; Roy, A. D.; Ivanov, I. N.; Cao, D. A General Synthesis Approach for Supported Bimetallic Nanoparticles via Surface Inorganometallic Chemistry. *Science* **2018**, *362*, 560−564.
(28) Du, Y.-P.; Luterbacher, J. S. Designing Heterogeneous Catalysts for Renewable Catalysis Applications Using Metal Oxide Deposition. *Chim. Int. J. Chem.* **2019**, *73*, 698−706.
(29) Cheng, N.; Banis, M. N.; Liu, J.; Riese, A.; Li, X.; Li, R.; Ye, S.; Knights, S.; Sun, X. Extremely Stable Platinum Nanoparticles Encapsulated in a Zirconia Nanocage by Area-Selective Atomic Layer Deposition for the Oxygen Reduction Reaction. *Adv. Mater.* **2015**, *27*, 277−281.
(30) Liu, S.; Tan, J. M.; Gulec, A.; Crosby, L. A.; Drake, T. L.; Schweitzer, N. M.; Delferro, M.; Marks, L. D.; Marks, T. J.; Stair, P. C. Stabilizing Single-Atom and Small-Domain Platinum via Combining Organometallic Chemisorption and Atomic Layer Deposition. *Organometallics* **2017**, *36*, 818−828.
(31) Toebes, M. L.; van Dillen, J. A.; de Jong, K. P. Synthesis of Supported Palladium Catalysts. *J. Mol. Catal. Chem.* **2001**, *173*, 75−98.
(32) Kim, M.-Y.; Kyriakidou, E. A.; Choi, J.-S.; Toops, T. J.; Binder, A. J.; Thomas, C.; Parks, J. E.; Schwartz, V.; Chen, J.; Hensley, D. K. Enhancing low-temperature activity and durability of Pd-based diesel oxidation catalysts using ZrO2 supports. *Appl. Catal., B* **2016**, *187*, 181−194.
(33) Lu, J.; Liu, B.; Greeley, J. P.; Feng, Z.; Libera, J. A.; Lei, Y.; Bedzyk, M. J.; Stair, P. C.; Elam, J. W. Porous Alumina Protective Coatings on Palladium Nanoparticles by Self-Poisoned Atomic Layer Deposition. *Chem. Mater.* **2012**, *24*, 2047−2055.
(34) Onn, T. M.; Zhang, S.; Arroyo-Ramirez, L.; Chung, Y.-C.; Graham, G. W.; Pan, X.; Gorte, R. J. Improved Thermal Stability and Methane-Oxidation Activity of Pd/Al2O3 Catalysts by Atomic Layer Deposition of ZrO2. *ACS Catal.* **2015**, *5*, 5696−5701.
(35) Zhu, G.; Han, J.; Zemlyanov, D. Y.; Ribeiro, F. H. The Turnover Rate for the Catalytic Combustion of Methane over Palladium Is Not Sensitive to the Structure of the Catalyst. *J. Am. Chem. Soc.* **2004**, *126*, 9896−9897.
(36) Park, J.-H.; Cho, J. H.; Kim, Y. J.; Kim, E. S.; Han, H. S.; Shin, C.-H. Hydrothermal stability of Pd/ZrO2 catalysts for high temperature methane combustion. *Appl. Catal., B* **2014**, *160*−*161*, 135−143.
(37) Hackett, S. F. J.; Brydson, R. M.; Gass, M. H.; Harvey, I.; Newman, A. D.; Wilson, K.; Lee, A. F. High-Activity, Single-Site Mesoporous Pd/Al2O3 Catalysts for Selective Aerobic Oxidation of Allylic Alcohols. *Angew. Chem.* **2007**, *119*, 8747−8750.
(38) Kattel, S.; Liu, P.; Chen, J. G. Tuning Selectivity of CO2 Hydrogenation Reactions at the Metal/Oxide Interface. *J. Am. Chem. Soc.* **2017**, *139*, 9739−9754.
(39) Graciani, J.; Mudiyanselage, K.; Xu, F.; Baber, A. E.; Evans, J.; Senanayake, S. D.; Stacchiola, D. J.; Liu, P.; Hrbek, J.; Sanz, J. F.; Rodriguez, J. A. Highly active copper-ceria and copper-ceria-titania catalysts for methanol synthesis from CO2. *Science* **2014**, *345*, 546−550.
(40) Calaza, F.; Stiehler, C.; Fujimori, Y.; Sterrer, M.; Beeg, S.; Ruiz-Oses, M.; Nilius, N.; Heyde, M.; Parviainen, T.; Honkala, K.; Häkkinen, H.; Freund, H.-J. Carbon Dioxide Activation and Reaction Induced by Electron Transfer at an Oxide-Metal Interface. *Angew. Chem., Int. Ed.* **2015**, *54*, 12484−12487.
(41) Rodriguez, J. A.; Liu, P.; Stacchiola, D. J.; Senanayake, S. D.; White, M. G.; Chen, J. G. Hydrogenation of CO2 to Methanol: Importance of Metal-Oxide and Metal-Carbide Interfaces in the Activation of CO2. *ACS Catal.* **2015**, *5*, 6696−6706.
(42) Kwak, J. H.; Kovarik, L.; Szanyi, J. Heterogeneous Catalysis on Atomically Dispersed Supported Metals: CO2 Reduction on Multifunctional Pd Catalysts. *ACS Catal.* **2013**, *3*, 2094−2100.
(43) Park, J.-N.; McFarland, E. W. A highly dispersed Pd-Mg/SiO2 catalyst active for methanation of CO2. *J. Catal.* **2009**, *266*, 92−97.
(44) Wang, X.; Shi, H.; Kwak, J. H.; Szanyi, J. Mechanism of CO2 Hydrogenation on Pd/Al2O3 Catalysts: Kinetics and Transient DRIFTS-MS Studies. *ACS Catal.* **2015**, *5*, 6337−6349.
(45) Bibby, D. M.; Howe, R. F.; McLellan, G. D. Coke Formation in High-Silica Zeolites. *Appl. Catal. Gen.* **1992**, *93*, 1−34.
(46) Wang, J.; Li, G.; Li, Z.; Tang, C.; Feng, Z.; An, H.; Liu, H.; Liu, T.; Li, C. A highly selective and stable ZnO-ZrO 2 solid solution catalyst for CO 2 hydrogenation to methanol. *Sci. Adv.* **2017**, *3*, No. e1701290.
(47) Samson, K.; Śliwa, M.; Socha, R. P.; Góra-Marek, K.; Mucha, D.; Rutkowska-Zbik, D.; Paul, J.-F.; Ruggiero-Mikołajczyk, M.; Grabowski, R.; Słoczyński, J. Influence of ZrO2 Structure and Copper Electronic State on Activity of Cu/ZrO2 Catalysts in Methanol Synthesis from CO2. *ACS Catal.* **2014**, *4*, 3730−3741.
(48) Li, K.; Chen, J. G. CO2 Hydrogenation to Methanol over ZrO2-Containing Catalysts: Insights into ZrO2 Induced Synergy. *ACS Catal.* **2019**, *9*, 7840−7861.
(49) Petrov, A. W.; Ferri, D.; Tarik, M.; Kröcher, O.; van Bokhoven, J. A. Deactivation Aspects of Methane Oxidation Catalysts Based on Palladium and ZSM-5. *Top. Catal.* **2017**, *60*, 123−130.
(50) Moulijn, J. A.; van Diepen, A. E.; Kapteijn, F. Catalyst deactivation: is it predictable? *Appl. Catal. Gen.* **2001**, *212*, 3−16.
(51) Hu, K.-J.; Plant, S. R.; Ellis, P. R.; Brown, C. M.; Bishop, P. T.; Palmer, R. E. Atomic Resolution Observation of a Size-Dependent Change in the Ripening Modes of Mass-Selected Au Nanoclusters Involved in CO Oxidation. *J. Am. Chem. Soc.* **2015**, *137*, 15161−15168.
(52) Gilroy, K. D.; Elnabawy, A. O.; Yang, T.-H.; Roling, L. T.; Howe, J.; Mavrikakis, M.; Xia, Y. Thermal Stability of Metal Nanocrystals: An Investigation of the Surface and Bulk Reconstructions of Pd Concave Icosahedra. *Nano Lett.* **2017**, *17*, 3655−3661.
(53) O'Neill, B. J.; Jackson, D. H. K.; Crisci, A. J.; Farberow, C. A.; Shi, F.; Alba-Rubio, A. C.; Lu, J.; Dietrich, P. J.; Gu, X.; Marshall, C. L.; Stair, P. C.; Elam, J. W.; Miller, J. T.; Ribeiro, F. H.; Voyles, P. M.; Greeley, J.; Mavrikakis, M.; Scott, S. L.; Kuech, T. F.; Dumesic, J. A. Stabilization of Copper Catalysts for Liquid-Phase Reactions by Atomic Layer Deposition. *Angew. Chem., Int. Ed.* **2013**, *52*, 13808−13812.
(54) Álvarez Galván, C.; Schumann, J.; Behrens, M.; Fierro, J. L. G.; Schlögl, R.; Frei, E. Reverse Water-Gas Shift Reaction at the Cu/ZnO Interface: Influence of the Cu/Zn Ratio on Structure-Activity Correlations. *Appl. Catal., B* **2016**, *195*, 104−111.
(55) Bahmanpour, A. M.; Héroguel, F.; Kılıç, M.; Baranowski, C. J.; Artiglia, L.; Röthlisberger, U.; Luterbacher, J. S.; Kröcher, O. Cu-Al Spinel as a Highly Active and Stable Catalyst for the Reverse Water Gas Shift Reaction. *ACS Catal.* **2019**, *9*, 6243−6251.
(56) Aitbekova, A.; Wu, L.; Wrasman, C. J.; Boubnov, A.; Hoffman, A. S.; Goodman, E. D.; Bare, S. R.; Cargnello, M. Low-Temperature Restructuring of CeO2-Supported Ru Nanoparticles Determines Selectivity in CO2 Catalytic Reduction. *J. Am. Chem. Soc.* **2018**, *140*, 13736−13745.
(57) Chen, X.; Su, X.; Su, H.-Y.; Liu, X.; Miao, S.; Zhao, Y.; Sun, K.; Huang, Y.; Zhang, T. Theoretical Insights and the Corresponding Construction of Supported Metal Catalysts for Highly Selective CO2 to CO Conversion. *ACS Catal.* **2017**, *7*, 4613−4620.
(58) Matsubu, J. C.; Yang, V. N.; Christopher, P. Isolated Metal Active Site Concentration and Stability Control Catalytic CO2 Reduction Selectivity. *J. Am. Chem. Soc.* **2015**, *137*, 3076−3084.
(59) Wang, C.; Guan, E.; Wang, L.; Chu, X.; Wu, Z.; Zhang, J.; Yang, Z.; Jiang, Y.; Zhang, L.; Meng, X.; Gates, B. C.; Xiao, F.-S. Product Selectivity Controlled by Nanoporous Environments in Zeolite Crystals Enveloping Rhodium Nanoparticle Catalysts for CO2 Hydrogenation. *J. Am. Chem. Soc.* **2019**, *141*, 8482−8488.
(60) Matsubu, J. C.; Zhang, S.; DeRita, L.; Marinkovic, N. S.; Chen, J. G.; Graham, G. W.; Pan, X.; Christopher, P. Adsorbate-mediated strong metal-support interactions in oxide-supported Rh catalysts. *Nat. Chem.* **2017**, *9*, 120−127.

https://dx.doi.org/10.1021/acscatal.0c02146
ACS Catal. 2020, 10, 12058−12070

(61) Cerrato, G.; Bordiga, S.; Barbera, S.; Morterra, C. Surface characterization of monoclinic ZrO2. *Appl. Surf. Sci.* **1997**, *115*, 53−65.
(62) Wang, Y. H.; Gao, W. G.; Wang, H.; Zheng, Y. E.; Na, W.; Li, K. Z. Structure-activity relationships of Cu-ZrO2 catalysts for CO2 hydrogenation to methanol: interaction effects and reaction mechanism. *RSC Adv.* **2017**, *7*, 8709−8717.
(63) Kattel, S.; Yan, B.; Yang, Y.; Chen, J. G.; Liu, P. Optimizing Binding Energies of Key Intermediates for CO2 Hydrogenation to Methanol over Oxide-Supported Copper. *J. Am. Chem. Soc.* **2016**, *138*, 12440−12450.
(64) Bhattacharyya, K.; Danon, A.; K.Vijayan, B.; Gray, K. A.; Stair, P. C.; Weitz, E. Role of the Surface Lewis Acid and Base Sites in the Adsorption of CO2 on Titania Nanotubes and Platinized Titania Nanotubes: An in Situ FT-IR Study. *J. Phys. Chem. C* **2013**, *117*, 12661−12678.
(65) Ren, J.; Guo, H.; Yang, J.; Qin, Z.; Lin, J.; Li, Z. Insights into the mechanisms of CO2 methanation on Ni(111) surfaces by density functional theory. *Appl. Surf. Sci.* **2015**, *351*, 504−516.
(66) Huygh, S.; Bogaerts, A.; Neyts, E. C. How Oxygen Vacancies Activate CO2Dissociation on TiO2Anatase (001). *J. Phys. Chem. C* **2016**, *120*, 21659−21669.
(67) Zhang, X.; Zhu, X.; Lin, L.; Yao, S.; Zhang, M.; Liu, X.; Wang, X.; Li, Y.-W.; Shi, C.; Ma, D. Highly Dispersed Copper over *β*-Mo2C as an Efficient and Stable Catalyst for the Reverse Water Gas Shift (RWGS) Reaction. *ACS Catal.* **2017**, *7*, 912−918.
(68) Baxter, E. T.; Ha, M.-A.; Cass, A. C.; Alexandrova, A. N.; Anderson, S. L. Ethylene Dehydrogenation on Pt4,7,8 Clusters on Al2O3: Strong Cluster Size Dependence Linked to Preferred Catalyst Morphologies. *ACS Catal.* **2017**, *7*, 3322−3335.

https://dx.doi.org/10.1021/acscatal.0c02146
ACS Catal. 2020, 10, 12058−12070